Korean J. Chem. Eng., 40(5), 1094-1102 (2023)
DOI: 10.1007/s11814-022-1274-1

pISSN: 0256-1115
eISSN: 1975-7220

Mechanism of sulfamethoxazole adsorption on wastewater-sludge-based biochar: Sludge type and modification improvement

Yongkui Yang*,†, Yifeng Ling*, Longfei Wang*, Peizhe Sun*, Lin Zhao*, and Hongyang Wang,†**

*School of Environmental Science and Engineering, Tianjin University, Tianjin 300072, China
**State Key Laboratory of Environmental Criteria and Risk Assessment, Chinese Research Academy of Environmental Sciences, Beijing 100012, China
(*Received 31 May 2022 • Revised 6 August 2022 • Accepted 24 August 2022*)

Abstract−With rapid industrialization and population growth, sewage sludge generation has increased worldwide, and it needs to be treated properly. The pyrolysis of sewage sludge into biochar provides sustainable benefits for concomitant pollutant adsorption and waste treatment. Sulfamethoxazole (SMX) antibiotics are highly prevalent in wastewater owing to their widespread utilization and low metabolic rate and removal efficiency during conventional wastewater treatment. Biochar is known to effectively remove pollutants from wastewater. However, the adsorption capacity and mechanism of SMX adsorption onto sludge-based biochar are currently unclear. Therefore, the adsorption behavior of SMX on sludge-based biochar from three sources (raw sludge, compost sludge, and digested sludge) and $ZnCl_2$-modified biochar was investigated. Among the unmodified biochars, raw sludge-based biochar exhibited the highest adsorption capacity, followed by compost sludge-based and digested sludge-based biochar. The pore-forming effect of $ZnCl_2$ application significantly increased the biochar specific surface area, which increased the equilibrium adsorption of SMX from 6.1 mg/g to 49.3 mg/g. The adsorption mechanisms involved electrostatic interactions, pore filling, hydrophobic interactions, hydrogen bonding, and π-π interactions. The findings of this study demonstrate the development of sewage sludge biochar and its effectiveness for the treatment of antibiotics containing wastewater.

Keywords: Biochar, Sludge Type, $ZnCl_2$ Modification, Adsorption, Sulfamethoxazole (SMX)

INTRODUCTION

Antibiotics, mainly sulfonamides, tetracyclines, macrolides, and quinolones [1], are extensively used to protect human and livestock health by preventing and controlling bacterial infections [2]. Among them, sulfamethoxazole (SMX) has been widely detected in rivers and lakes (0.2-2.8 μg/L) [3], hospital wastewater (0.2-27.8 μg/L), municipal wastewater (0.4-7.9 μg/L) [4], mariculture water (0.04-5.6 mg/L) [5], and pharmaceutical industry effluent (~18 mg/L) [6]. Hence, efficient SMX removal from wastewater is necessary to limit its direct threat to microorganisms and the propagation of antibacterial resistance genes [7].

Current technologies for antibiotics removal include adsorption, membrane filtration, and biodegradation [8]. Adsorption is a widely used treatment process with practical applications owing to its high efficiency, simple operation, and low energy consumption [9], which eliminates the contaminants through a surface-based phenomenon that attracts pollutant molecules, atoms, or ions onto the surface of absorbents [10,11]. Biochar is a preferable adsorbent compared to commercial activated carbon owing to its low cost, wide availability of raw materials, and low environmental impact [10,12,13]. Previous studies have examined antibiotics removal using biochar that was mainly produced by pyrolysis of agricultural biowastes, such as microalgae [14], wheat straw [15], pine sawdust [16], apple trees waste [17], and lignocellulosic biomass [18]. However, studies on antibiotics removal using biochar derived from sewage sludge are limited.

China has over 4,000 operational wastewater treatment plants owing to the increasing wastewater generation resulting from the population growth and industrial development [19]. More than 60 million tons of municipal sludge was produced in China by 2020. For decades, landfilling has been the main sludge treatment and disposal strategy, whereas composting and anaerobic digestion are increasingly used to produce energy from sludge. Recently, the carbonization of sludge has gained extensive attention because of its abundant functional groups, high organic content, and higher biochar yield [9]. However, limited studies have reported the use of sludge-based biochar for antibiotic adsorption. Further, previous studies only focused on biochar from the pyrolysis of raw sewage sludge [9,20]. The characteristics of sewage sludge are altered after different treatments, such as aerobic composting and anaerobic digestion. The different constituents of sludge can also affect the properties of the biochar produced [21,22]. However, differences in the adsorption capacity of the biochar produced from aerobically composted and anaerobically digested sludge remain unclear.

Biochar prepared through pyrolytic carbonization exhibits poor adsorption capacity with underdeveloped pore architecture and a low surface area [23], limiting large-scale application. Therefore, activation and structural modification are essential to improve its physiochemical properties and adsorption capacity [14]. Several tech-

†To whom correspondence should be addressed.
E-mail: ykyang@tju.edu.cn, wanghongyang_why@126.com

niques have been used for adsorbent modification, such as acid/base treatment [24], carbon nanotubes loading [25], and magnetic-activation [26]. Among various techniques, $ZnCl_2$ application leads to an apparent pore-forming effect during heat treatment [7], thus increasing the surface area and active sites for adsorption. However, the efficiency and mechanism of SMX adsorption on $ZnCl_2$-modified sludge biochar is yet to be elucidated.

The main objective of this study was to investigate the adsorption capacity and mechanism of SMX adsorption on unmodified biochar prepared from aerobically composted and anaerobically digested sludge, as well as $ZnCl_2$-modified biochar. We investigated (1) the SMX adsorption behavior of three types of sludge biochar produced from raw sludge, compost sludge, and digested sludge; (2) biochar adsorption capacity improvement after modification with $ZnCl_2$; and (3) the adsorption mechanism of SMX on biochar using adsorption kinetics, isotherm, thermodynamics, and influencing factor analysis. This study provides a valuable perspective on the economic utilization of sludge and the efficient removal of antibiotics from wastewater.

MATERIALS AND METHODS

1. Chemicals and Materials

Sulfamethoxazole (SMX 99.7%) and Zinc chloride ($ZnCl_2$ 98%) were purchased from the Saan Chemical Technology Co. (Shanghai, China) and Fuchen Chemical Reagent Co. (Tianjin, China), respectively. Raw, digested, and compost sludge was collected from a municipal wastewater sludge treatment plant operating anaerobic digestion and aerobic composting processes in Tianjin, China. Ultrapure water (18 MΩ/cm) was used in the experiments.

2. Preparation of Sludge-based Biochar

The three types of sludge were air-dried and pulverized to pass through a 60-mesh screen, followed by pyrolysis in a vacuum atmosphere tube furnace (SK-G 04123K, Zhonghuan Electric Furnace Co., China) at 800 °C for 2 h under N_2 flow [24]. After cooling to room temperature (25 °C), the pyrolyzed samples were washed with ultrapure water with agitation for 3 h, and this operation was repeated thrice. Finally, raw sludge-based biochar (RSB), compost sludge-based biochar (CSB), and digested sludge-based biochar (DSB) were obtained after drying at 105 °C for 12 h and sieved through a 100-mesh screen for the experiments. For modifying biochar, the RSB was immersed in 3 mol/L $ZnCl_2$ solution in a water bath shaker (SHZ-B, Boxunsh, China) at 80 °C for 12 h, then dried in an oven (FXB202-00, Shuliyiqi, China) at 105 °C. Subsequently, the sludge was pyrolyzed, as described above. The cooled sample was washed thrice with hydrochloric acid at 1 h intervals to remove residual zinc [27]. Finally, the Zn-modified RSB (Zn-RSB) was obtained after drying and sieving.

3. Adsorption Experiments

Biochar (0.015 g) was added to 30 mL of SMX solution (1 and 50 mg/L) for the adsorption kinetics studies. The adsorption was carried out in a constant temperature oscillator (150 rpm, 25 °C) at pH 7 for 72 h in the dark. The adsorption isotherm experiments were conducted using 30-200 mg/L SMX, with the solutions shaken at 150 rpm for 72 h to achieve equilibrium. Additionally, the effect of the solution pH on SMX adsorption on biochar was examined at pH 2-11. The effects of biochar dosage (0.5, 1.0, 2.0, and 3.0 mg/L) and temperature (25, 35, and 45 °C) on SMX adsorption were studied. All experiments were performed in duplicate.

The adsorption capacity was calculated as follows [28]:

$$q_t = \frac{(C_0 - C_t)V}{W} \quad (1)$$

where C_0 and C_t (mg/L) are the concentrations of SMX initially and time t (h), respectively, V (L) is the volume of antibiotic solution, W (g) is the mass of the biochar, and q_t represents the adsorption capacity at time t.

The pseudo-first-order (Eq. (2)) and pseudo-second-order (Eq. (3)) models were used to evaluate the adsorption capacity of the biochar for SMX at different time intervals. The equations and linear relationships are as follows [28,29]:

$$\ln(q_e - q_t) = \ln q_e - k_1 t \quad (2)$$

$$\frac{t}{q_t} = \frac{1}{k_2 q_e^2} + \frac{t}{q_e} \quad (3)$$

where q_e (mg/g) is the adsorption capacity of the biochar at equilibrium, and k_1 (min^{-1}) and k_2 (g/(mg·min)) are the rate constants of pseudo-first-order and pseudo-second-order models, respectively.

The Langmuir (Eq. (4)) and Freundlich (Eq. (5)) adsorption isotherm models hypothesize that the adsorption process is monolayer adsorption on a homogeneous surface and multilayer adsorption on non-homogeneous surfaces, respectively [30,31]. The equations and linear relationships are as follows:

$$\frac{1}{q_e} = \frac{1}{K_L C_e q_m} + \frac{1}{q_m} \quad (4)$$

$$\ln q_e = \ln k_F + \frac{1}{n_F} \ln C_e \quad (5)$$

where C_e (mg/L) is the concentration of SMX at equilibrium, q_m (mg/g) is the theoretical maximum adsorption capacity of the biochar for SMX, and K_L (L/mg) is the Langmuir constant related to the adsorption energy. n_F and K_F ($mg^{1-1/n}$ $L^{1/n}$/g) are Freundlich constants related to the intensity and capacity of the adsorption process, respectively.

For a better understanding of the adsorption of SMX on Zn-RSB, thermodynamic models were investigated [29]. The change in Gibbs free energy (ΔG (kJ/mol)), entropy (ΔS (kJ/(mol·K))), and enthalpy (ΔH (kJ/mol)) were determined using the calculations as follows (Eqs. (6)-(7)):

$$\Delta G = -RT \ln K_L \quad (6)$$

$$\Delta G = \Delta H - T\Delta S \quad (7)$$

where R is the universal gas constant (8.314 J/(mol·K)), T (K) is the absolute temperature of system, and K_L (L/mol) represents the thermodynamic equilibrium constant.

4. Characterization of Sludge-based Biochar and other Analysis

The biochar morphology was characterized using scanning electron microscopy (SEM, Gemini SEM 500, Zeiss, Germany) at 20.0 kV with a magnification of 10,000×. X-ray photoelectron spectroscopy (XPS, ESCALAB 250Xi, Thermo Scientific, USA) was per-

formed to analyze the surface elements and their valence states (Al Kα radiation source, passage energy of 40 eV, step length of 0.1 eV). The surface area, pore volume, and porosity of the adsorbents were determined using the Brunauer-Emmett-Teller analysis (BET, ASAP2020, Micromeritics, USA). Fourier transform infrared spectroscopy (FTIR, ALPHA, Bruker, Germany) of the adsorbents was performed in the range of 400-4,000 cm^{-1}. X-ray diffraction (XRD, SmartLab, Rigaku, Japan) was performed using Cu Kα as the radiation source and the crystal structures were analyzed at a diffraction angle of 5-90°, with a scanning rate of 5° min^{-1}. The zeta potential of the biochar samples was determined using a zeta potential analyzer (Zetasizer Nano ZS; Malvern, UK). The pH was determined using a pH meter (SevenCompact, Mettler Toledo, Switzerland). After filtering through a 0.22 μm filter, SMX concentration was determined using high-performance liquid chromatography (HPLC, LC-2030C 3D, Shimadzu, China) at 270 nm with a retention time of 4.0 min. The chromatographic column RX-C18 (150×4.6 mm; particle size 5.0 μm) was used and the mobile phase consisted of methanol and 0.01% phosphoric acid (v/v, 40 : 60) in isocratic mode at a flow rate of 1.0 mL/min.

RESULTS AND DISCUSSION

1. Characteristics of the Three Unmodified Sludge-based Biochars

SEM characterization (Fig. 1(a)-(c)) showed that the surfaces of the three unmodified sludge-based biochars were irregularly distributed with numerous pores and some crystal structures. Abundant pores were evident on the surfaces of RSB and CSB, and the number and diameter of pores were relatively similar on both adsorbent surfaces, while pores on the DSB surface were fewer. All biochars exhibited high specific surface area (S_{BET}, 83.1-105.5 m^2/g) and total pore volume (V_{tot}, 0.146-0.190 cm^3/g) (Table 1), indicating the presence of abundant binding sites for adsorption. C, O, N, and S, were the major elements detected on the surface of the three types of biochar (Table 1), where high C and O contents facilitated pore formation and hydrogen bond donors exhibiting great affinity for hydrophobic organic contaminants [22,25]. Additionally, the small differences between the (N+O)/C ratios of the three biochars indicated slight variations in the surface polarity and degree of aromatization [14]. The detailed peaks of C 1s and O 1s on biochars are seen in Fig. 2. C 1s shows that sludge biochars have a higher content of C-C/C=C (61.8-76.1%, 284.8 eV) and small amounts of C-O (17.8-31.1%, 286.4 eV) and C=O (6.1-8.8%, 289.2 eV) [32,33]. The FTIR spectra (Fig. 1(e)) of the three biochars were similar, indicating abundant active functional groups on their

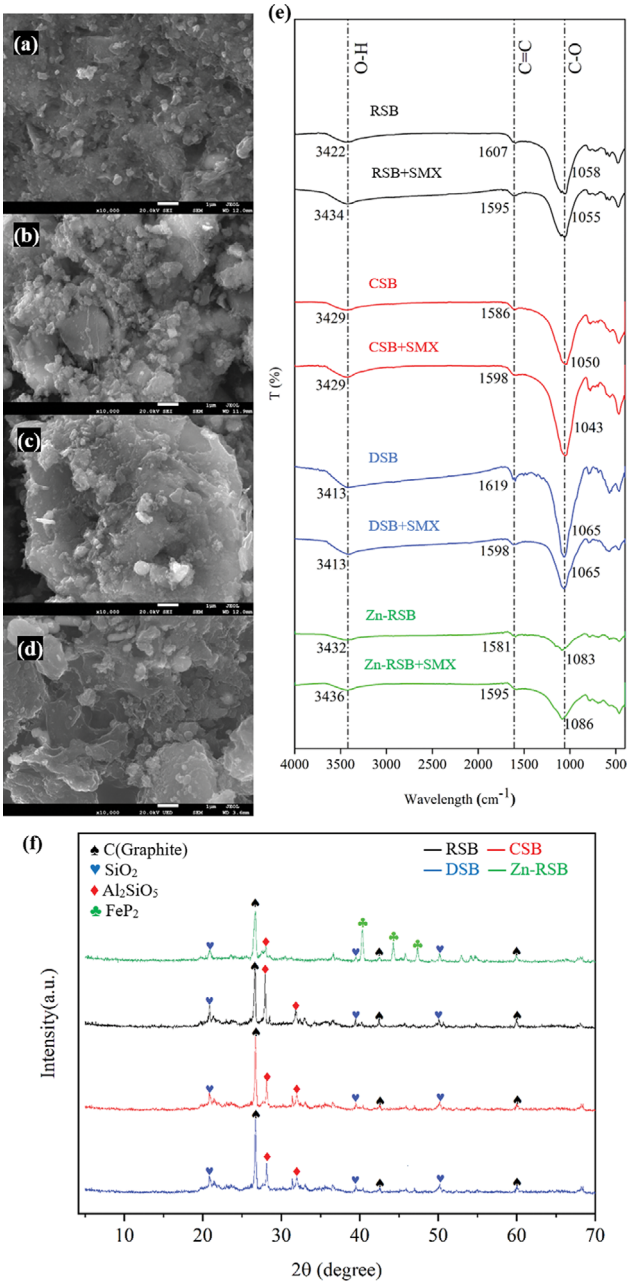

Fig. 1. SEM micrographs, FTIR and XRD spectra of sludge-based biochars: (a) RSB: raw sludge-based biochar; (b) CSB: composted sludge-based biochar; (c) DSB: digested sludge-based biochar; (d) Zn-RSB: Zn-modified raw sludge-based biochar; (e) FTIR analysis of biochar before and after SMX adsorption; (f) XRD spectra of the sludge-based biochars.

Table 1. Basic properties of the sludge-based biochars

Biochar	Porosity characteristic			Surface elements content (%)				Atomic ratio	Zeta potential (mV)
	S_{BET} (m^2/g)	D_p (nm)	V_{tot} (cm^3/g)	C	O	N	S	(N+O)/C	pH 7
RSB	105.5	7.2	0.190	49.3	45.3	4.3	1.1	1.0	−31.0
CSB	83.1	7.2	0.150	52.4	42.4	3.5	1.5	0.9	−33.5
DSB	97.3	6.0	0.146	58.4	34.9	4.3	2.4	0.7	−33.0
Zn-RSB	326.5	2.6	0.216	66.4	29.2	3.6	0.8	0.5	−36.1

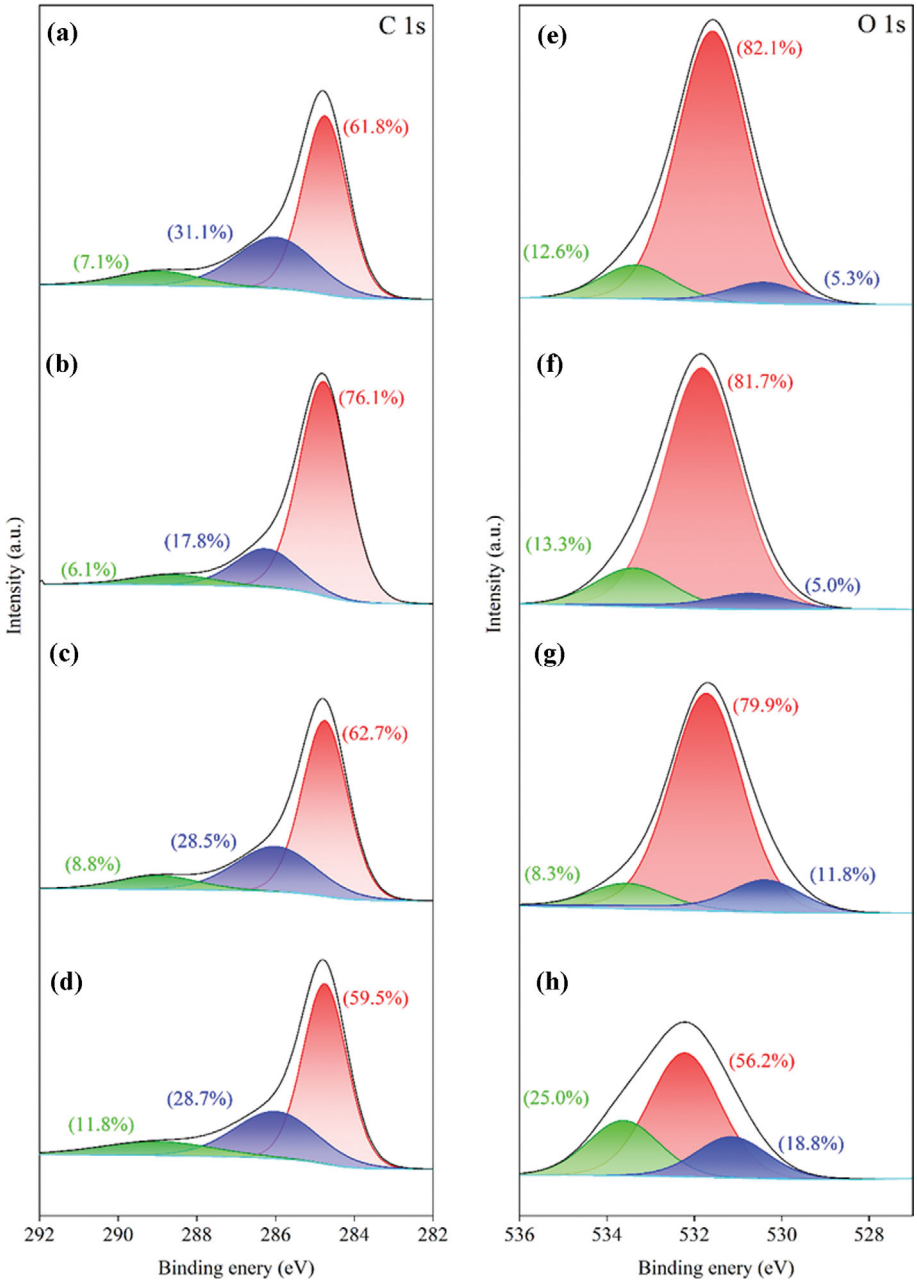

Fig. 2. XPS spectra of the C 1s (a)-(d) and O 1s (e)-(h) of the sludge-based biochars. (a), (e) RSB: raw sludge-based biochar; (b), (f) CSB: compost sludge-based biochar; (c), (g) DSB: digested sludge-based biochar; (d), (h) Zn-RSB: Zn-modified sludge-based biochar.

surfaces, with peaks of the O-H bond at 3,413-3,429 cm^{-1}, C=C bond at 1,586-1,619 cm^{-1} and C-O bond at 1,050-1,065 cm^{-1} [26, 34]. The XPS and FTIR spectra confirm the presence of various functional groups, such as -OH, C=C, C=O, O=C-O and C-O in sludge-based biochars. The differences in the intensity of these peaks could be attributed to changes in the functional groups contents in the sludge during the aerobic composting and anaerobic digestion processes [35]. All sludge-based biochars showed negative surface charge in solutions of pH 7 (Table 1) [21]. The XRD analysis (Fig. 1(f)) of the crystal structures showed that diffraction peaks at 26°, 42°, and 60°, indicating the presence of a graphite structure [25], which facilitated the formation of π-π conjugation between the aromatic rings of the biochar [34]. The diffraction peaks at 2θ= 21°, 39° and 50° are the characteristic peaks of quartz (SiO_2), while the diffraction peaks at 2θ=28° and 32° are the typical peaks of kyanite (Al_2SiO_5), both of which are crystals formed from silicate and aluminum salts in sludge biochar. These minerals may help to promote the formation of oxygenated functional groups, and also serve as natural pore-forming agents to form a hierarchical porous structure in the biochars [14].

2. SMX Adsorption on the Three Unmodified Sludge-based Biochars

2-1. Adsorption Kinetics

Fig. 3(a) presents the adsorbed concentration vs time plot for

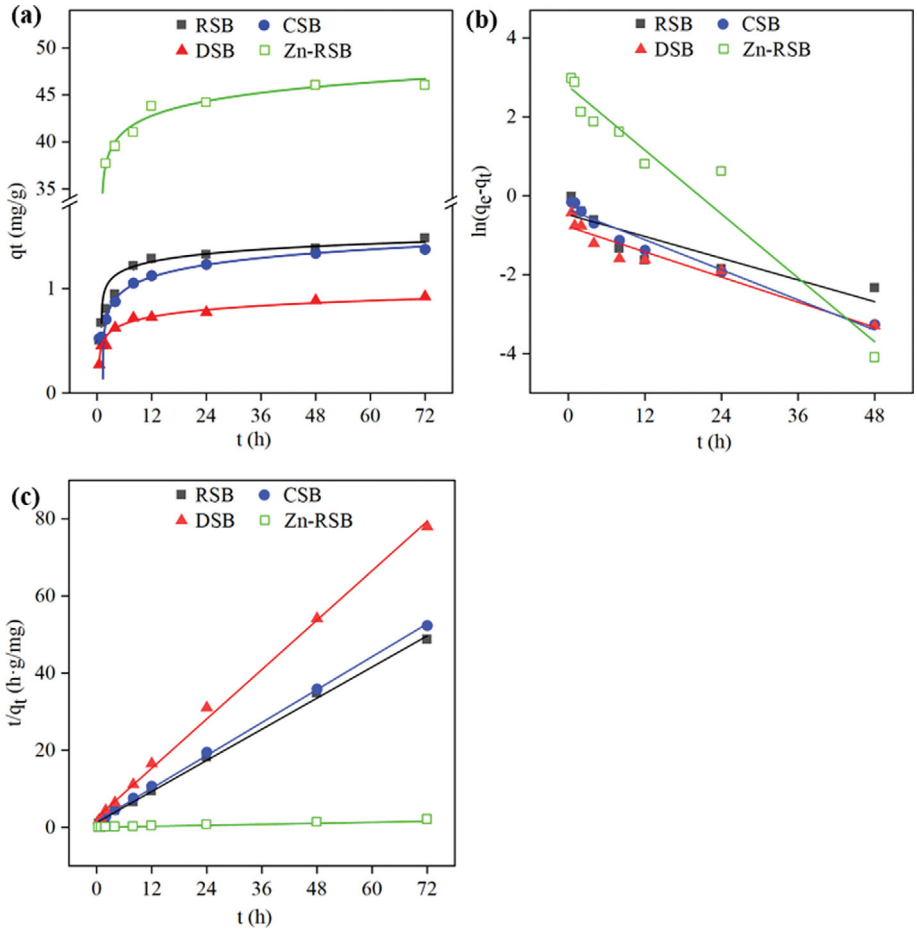

Fig. 3. Kinetic curves of SMX adsorption on sludge-based biochars: (a) Adsorption amount with time; (b) pseudo-first-order model; (c) pseudo-second- order model.

Table 2. Parameters of adsorption kinetics and adsorption isotherms curves

Biochar	Pseudo-first-order			Pseudo-second-order			Langmuir			Freundlich		
	K_1 (min^{-1})	$Q_{e(cal)}$ (mg/g)	R^2	K_2 (g/(mg·min))	$Q_{e(cal)}$ (mg/g)	R^2	k_L (L/mg)	q_m (mg/g)	R^2	k_F ($mg^{1-1/n}$ $L^{1/n}$/g)	n_F	R^2
RSB	0.046	0.618	0.772	0.362	1.487	0.998	0.522	6.1	0.998	1.992	2.689	0.970
CSB	0.064	0.704	0.963	0.323	1.405	0.999	0.553	5.1	0.996	1.926	3.192	0.988
DSB	0.053	0.456	0.925	0.455	0.947	0.997	0.304	4.3	0.992	1.140	2.493	0.992
Zn-RSB	0.135	16.035	0.948	0.031	46.512	0.999	0.698	49.3	0.999	22.790	4.978	0.946

SMX adsorption on the three biochars. The adsorbed SMX concentration increased rapidly during the first 12 h because of the abundant active sites, rich pore structure, high concentration gradient and weak internal diffusion resistance [26,36]. Thereafter, the SMX adsorption decreased as the active sites saturated and gradually reached equilibrium by 72 h. The SMX adsorbed on RSB at equilibrium was 1.48 mg/g, which was 1.1- and 1.6-fold higher than that on CSB and DSB, respectively. This may be attributed to the highest S_{BET}, V_{tot} (Table 1), and functional group complexation of RSB (Fig. 1-2). Based on the correlation coefficients, R^2 (Table 2), the pseudo-second-order model better describes the adsorption kinetic data for all three biochars (Fig. 3(b)-(c)). This implies that chemisorption involving valence forces or exchanging electrons can overcome the mass transfer resistance between the antibiotic and biochar [25].

2-2. Adsorption Isotherms

The Langmuir isotherm model better represented the adsorption data than the Freundlich model (Fig. 4), indicating that the SMX adsorption process was consistent with monolayer adsorption on a homogeneous surface [37]. RSB exhibited the maximum SMX adsorption capacity (q_m, 6.1 mg/g), followed by that on CSB (5.1 mg/g) and DSB (4.3 mg/g) (Table 2). The adsorption capacity of the three sludge-based biochars was higher than that of coffee ground biochar (0.1 mg/g) [38], but less than that of magnetic modified pine sawdust biochar (13.8 mg/g) [39]. The K_L values were all <1, indicating that the SMX adsorption process was favor-

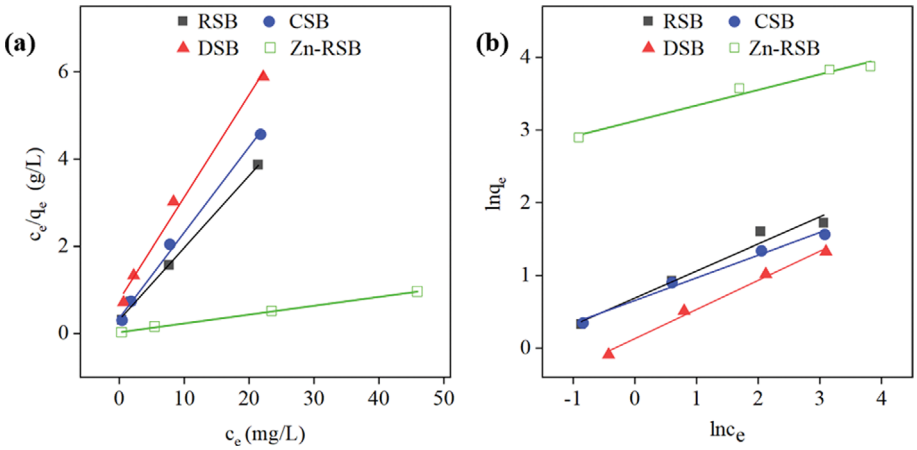

Fig. 4. Isotherm fitting curves of SMX adsorption on sludge-based biochars: (a) Langmuir and (b) Freundlich.

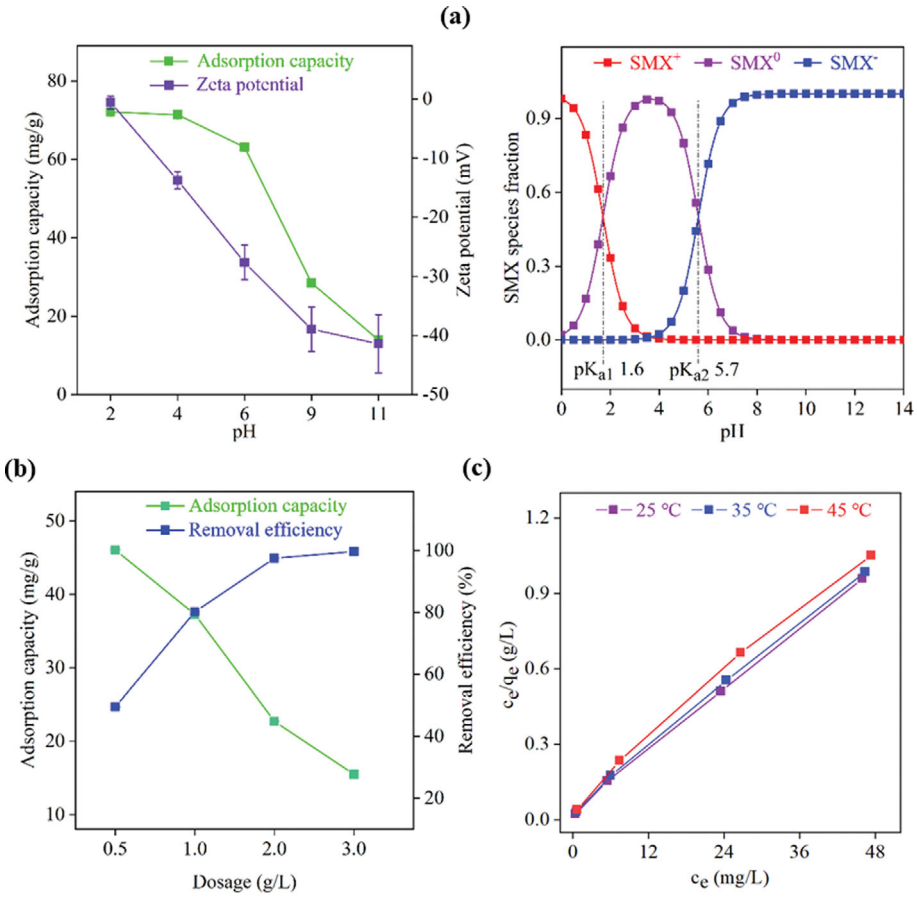

Fig. 5. Effect of (a) pH, (b) adsorbent dosage, and (c) temperature on SMX adsorption on Zn-RSB.

able [38]. The heterogeneity factors of $1<n_F<10$ indicated a strong affinity between the adsorbent and adsorbate [26], suggesting that the biochars were effective for SMX removal from water.

3. SMX Adsorption on Zn-modified Sludge-based Biochar

3-1. Adsorption Kinetics and Isotherms

Raw sludge-based biochar exhibited the highest adsorption capacity among the three unmodified biochars and was selected for modification using Zn for further adsorption analysis. Fig. 3(a) shows that SMX adsorption trend on biochar before and after modification was similar. The pseudo-second-order model described the experimental kinetic data better (Fig. 3(b)-(c)), and the adsorption data fitted the Langmuir isotherm better than the Freundlich isotherm (Fig. 4). As presented in Fig. 1(e) and Fig. 2, the FTIR and XPS spectra of Zn-RSB were similar to those of RSB, indicating that the functional groups composition of biochar did not change considerably after modification [20]. A similar phenome-

non was observed for crawfish shell biochar after $ZnCl_2$ modification [40]. In contrast, the maximum adsorption capacity of Zn-RSB at 49.3 mg/g was 8.1-fold higher than that before modification.

3-2. Effect of Different Parameters on SMX Adsorption

3-2-1. pH

Fig. 5(a) shows that with increasing pH, the Zn-RSB adsorption capacity decreased considerably, while the absolute zeta potential value increased. Zn-RSB exhibited higher SMX adsorption under acidic conditions similar to the SMX adsorption on magnetic-activated carbon composites [26]. At pH 2, close to the SMX pK_{a1} of 1.6 (Fig. 5(a)), Zn-RSB exhibited the maximum SMX adsorption of 72.1 mg/g, which is attributed to the π^{+}-π electron donor-acceptor (EDA) interactions between the protonated aniline ring on SMX and the rich π-electron surface of Zn-RSB [22]. These interactions intensified at a lower pH [41]. At pH 4-6, SMX adsorption decreased by 8.3 mg/g, which was likely caused by the increase in negative species (SMX^{-}) and negative charge on the biochar, which strengthened the electrostatic repulsion [42]. At pH 9, the substantially lower adsorption (28.5 mg/g) can be attributed to the enhanced electrostatic repulsion caused by abundant SMX [18] and the significant inhibition of hydrophobic interactions between SMX and the adsorbent, arising from the increase in pH and ionization [26]. A similar pH effect has been observed for the adsorption of SMX on carbon nanotube-modified sludge biochar [25].

3-2-2. Adsorbent Dosage

Fig. 5(b) shows the remarkable enhancement of SMX removal with an increasing adsorbent dosage. The highest removal efficiency (99.6%) was obtained at a dosage of 3.0 g/L, which was attributed to extensive active sites elicited by rich surface functional groups and the large available contact area [34]. However, the SMX adsorbed quantity decreased by 30.6 mg/g when the adsorbent dosage increased to 3.0 g/L, which can be attributed to the aggregation or overlap of active sites and an increase in the diffusion path length at high adsorbent doses [18].

3-2-3. Temperature

Fig. 5(c) shows the effect of temperature on the SMX adsorption on Zn-RSB. The negative values of ΔG (−30.0 to −30.4 kJ/mol) indicate that the adsorption was a spontaneous process. In addition, ΔG decreased with increasing T, indicating that a lower temperature favors higher SMX adsorption [43]. The positive ΔS value (0.020 kJ/mol) suggests an increase in the randomness of the solid/solution interface throughout SMX adsorption [18]. The value of ΔH was −23.95 kJ/mol, indicating an exothermic adsorption process [44], which is similar to the SMX adsorption on activated carbon [44]. In addition, the low absolute ΔH approached the magnitude of typical hydrogen bonding adsorption strengths (2-40 kJ/mol), suggesting a dominant role of hydrogen bonding interactions [45].

4. Mechanisms of Adsorption on Unmodified and Zn-modified Sludge-based Biochars

Fig. 6 shows the potential mechanisms of SMX adsorption on the unmodified and Zn-modified sludge biochars. The surfaces of the three unmodified sludge-based biochars are irregular, with a large specific surface area and total pore volume (Fig. 1(a)-(c) and Table 1), which provide substantial active sites and a low spatial potential resistance for SMX adsorption [46]. Among the three unmodified biochars, the lowest average pore diameter (D_p) and V_{tot} of DSB may have resulted in the lowest SMX adsorption, further proving that pore filling is an important mechanism [47]. XPS analysis of the biochars reveals (Fig. 2(a)-(c)) a high C=C content (61.8-76.1%) in C 1s peak that provided potential for forming π-π EDA between the biochar surface and aromatic ring of antibiotics [9,14]. Similarly, the benzene ring electrons as π-electron acceptors of hexadecyl trimethyl ammonium bromide-modified activated carbon were found to be bound by the amide and sulfonyl groups of SMX [44]. Meanwhile, a shift in the FTIR peak positions of the C=C groups (1,586-1,619 cm^{-1}) was observed after SMX adsorption on the three unmodified biochars (Fig. 1(e)), confirming that π-π EDA contributes to SMX adsorption [7,9]. The three peaks in XPS O 1s region (Fig. 2(e)-(g)) are associated with lattice

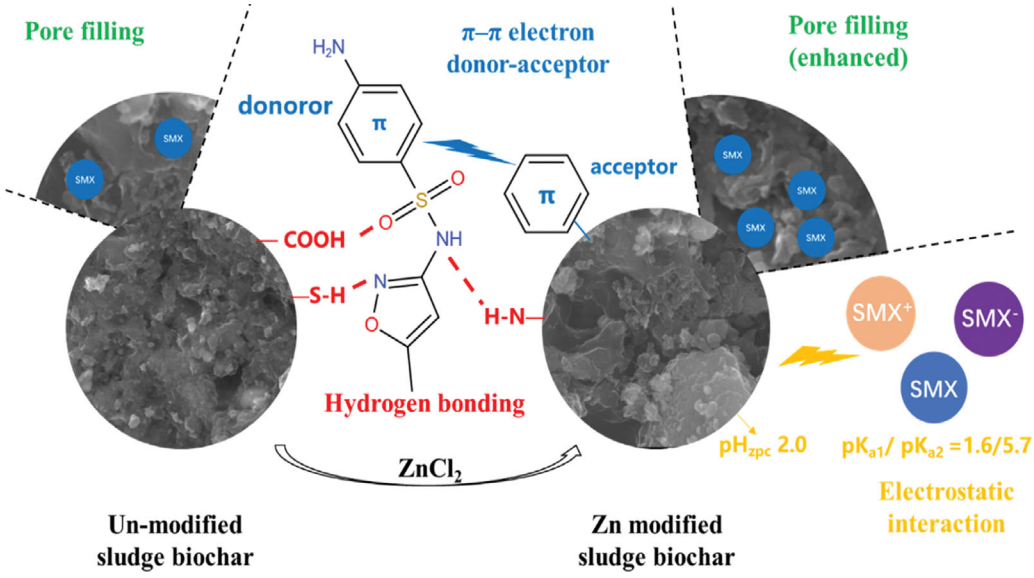

Fig. 6. Mechanisms of SMX adsorption on unmodified and modified sludge biochar.

oxygen in metal oxides (5.0-11.8%, 530.7 eV), vacancy oxygen (79.9-82.1%, 531.8 eV) and adsorbed oxygen (8.3-13.3%, 533.4 eV) [48-50], usually identified as C=O, O=C-O and C-O, respectively [46,50,51].

In FTIR, the shifts in the C-O, C=C and -OH stretching vibration peak at 1,050-1,058, 1,586-1,619 and 3,413-3,434 cm^{-1} were observed only for RSB after SMX adsorption, indicating the formation of hydrogen bonds between the -OH, and C-O groups of the biochar, and amino and sulfonyl groups of SMX [14,44]. However, these were only partially observed in CSB and DSB. The O content on the surfaces of RSB, CSB, and DSB decreased sequentially (Table 1), which is consistent with the decrease in the adsorbed SMX content. It indicates that the O content can contribute to the SMX adsorption capacity owing to the increased binding forces, such as hydrogen bonds [9]. In XPS O1s (Fig. 2(e)-(g)), RSB exhibited higher vacancy oxygen content than that in CSB and DSB, which can increase the oxygen adsorption sites for the chemisorbed oxygen on surface [49,50]. Wang et al. [52] using quantum chemical methods revealed that C=O and O=C-O groups can behave as active sites in penicillin adsorption, also demonstrating the important role of oxygen in the adsorption process. These characteristics reveal that the largest S_{BET}, V_{tot}, and functional group complexation of RSB contributed to higher SMX adsorption capacity than that of CSB and DSB. The pseudo-second-order kinetic and Langmuir models provided a good fit for SMX adsorption on the biochars (Table 2), indicating that monolayer chemisorption occurred during SMX removal [53].

After $ZnCl_2$ modification, the surface of Zn-RSB contained more pores (Fig. 1(d)), with 3.1- and 1.1-fold increase in the S_{BET} and V_{tot} values of RSB, respectively (Table 1), which was presumably correlated with the pore-building effect [27]. The increased surface S_{BET} of sludge-based biochar increases the number of active sites and consequently enhances the SMX adsorption [11,31]. The low D_p of Zn-RSB was consistent with previous studies on the modification of bamboo sawdust biochar [54] and antibiotic fermentation residue biochar [7], providing convincing evidence for the pore-forming process of $ZnCl_2$ that helps in hydrophobic interactions [14]. This mechanism observed for Zn-RSB suggests that the adsorption capacity is more dependent on the surface area of the biochar [22]. The XPS images illustrate that a small fraction of C-O bonds in RSB (Fig. 2(a)) was converted to C=O in Zn-RSB (Fig. 2(d)) by the dehydration effect of $ZnCl_2$ during carbonization [9], which may account for the peak shift of C-O peak (1,058 to 1,083 cm^{-1}) in FTIR (Fig. 1). Similar to carbon nanotube modified sludge-based biochars [25] and iron oxide-modified biochar from microalgae [55], XPS spectra reveal small amounts of C=O on the surfaces of sludge-based biochars, but the C=O peak was not observed in the FTIR. The FTIR spectra of Zn-RSB before and after SMX adsorption reveal shifts in the OH stretching vibration at 3,432 cm^{-1}, confirming hydrogen bonding between -COOH groups on the biochar surface and $-NH_2$, $-NO_2$ or hydrogen groups in SMX [56]. SMX adsorption on Zn-RSB was significantly affected by pH, indicating strong electrostatic and hydrophobic interactions between SMX and the biochar. The adsorption kinetics and isotherm behavior before and after the modification were consistent, suggesting that the adsorption mechanisms of Zn-RSB were similar to those of the unmodified biochars. Collectively, pore filling and hydrogen bonding are responsible for the differences in their adsorption capacity, while π-π EDA binding is the most prevalent mechanism for SMX adsorption on unmodified and Zn-modified sludge biochars [57].

CONCLUSIONS

This study investigated the SMX adsorption mechanism and capacity of unmodified biochars derived from three types of sludge and $ZnCl_2$-modified biochar. Based on their SMX adsorption capacity the sequence was raw sludge-based>compost sludge-based>digested sludge-based biochar, with a maximum SMX adsorption capacity of 6.1 mg/g. The adsorption kinetics were consistent with the pseudo-second-order model, and isothermal adsorption corresponds to the Langmuir monolayer adsorption model. The pore-forming effect of $ZnCl_2$ modification significantly increased the specific surface area of biochar, and consequently enhanced the equilibrium SMX adsorption capacity to 49.3 mg/g. The adsorption mechanisms involved electrostatic interaction, pore filling, hydrophobic interaction, hydrogen bonding, and π-π interaction. This study provides a value-added resource utilization method for municipal sludge combined with economic benefits that can significantly enhance the removal of antibiotics from wastewater. Further studies to evaluate the immobilization effects of other challenging pollutants, such as heavy metals on sludge-based biochars during wastewater treatment, may contribute to alleviating critical environmental issues.

ACKNOWLEDGEMENT

This study was financially supported by the Key Research and Development Plan Project of Tianjin of China (No. 21YFSNSN00160) and National Natural Science Foundation of China (No. 21407112).

DECLARATION OF COMPETING INTEREST

The authors declare that they have no known competing financial interests or personal relationships that could have appeared to influence the work reported in this paper.

REFERENCES

1. F. Yu, Y. Li, S. Han and J. Ma, *Chemosphere*, **153**, 365 (2016).
2. T. T. Qin, Z. W. Wang, X. Y. Xie, C. R. Xie, J. M. Zhu and Y. Li, *Water Sci. Technol.*, **76**, 3307 (2017).
3. A. L. Batt, S. Kim and D. S. Aga, *Chemosphere*, **68**, 428 (2007).
4. W.-Y. Ouyang, J. Birkigt, H. H. Richnow and L. Adrian, *Environ. Sci. Technol.*, **55**, 271 (2021).
5. M. Zhao, X. Ma, X. Liao, S. Cheng, Q. Liu, H. Wang, H. Zheng, X. Li, X. Luo, J. Zhao, F. Li and B. Xing, *Chem. Eng. J.*, **430**, 133092 (2022).
6. Y.-B. Zhang, J. Zhou, Q.-M. Xu, J.-S. Cheng, Y.-L. Luo and Y.-J. Yuan, *Sci. Total Environ.*, **565**, 547 (2016).
7. Q. Wu, Y. Zhang, M.-h. Cui, H. Liu, H. Liu, Z. Zheng, W. Zheng,

C. Zhang and D. Wen, *J. Hazard. Mater.*, **426**, 127798 (2022).
8. J. Radjenovic and M. Petrovic, *J. Hazard. Mater.*, **333**, 242 (2017).
9. Y. Ma, M. Li, P. Li, L. Yang, L. Wu, F. Gao, X. Qi and Z. Zhang, *Bioresour. Technol.*, **319**, 124199 (2021).
10. M. Shabir, M. Yasin, M. Hussain, I. Shafiq, P. Akhter, A.-S. Nizami, B.-H. Jeon and Y.-K. Park, *J. Ind. Eng. Chem.*, **112**, 1 (2022).
11. M. Shabir, N. Shezad, I. Shafiq, I. M. Maafa, P. Akhter, K. Azam, A. Ahmed, S. H. Lee, Y.-K. Park and M. Hussain, *J. Ind. Eng. Chem.*, **105**, 539 (2022).
12. M. Inyang and E. Dickenson, *Chemosphere*, **134**, 232 (2015).
13. S. Valizadeh, S. S. Lee, K. Baek, Y. J. Choi, B.-H. Jeon, G. H. Rhee, K.-Y. Andrew Lin and Y.-K. Park, *Environ. Res.*, **200**, 111757 (2021).
14. X. N. Law, W. Y. Cheah, K. W. Chew, M. F. Ibrahim, Y.-K. Park, S.-H. Ho and P. L. Show, *Environ. Res.*, **204**, 111966 (2022).
15. L. Zhao, F. Yang, Q. Jiang, M. Zhu, Z. Jiang, Y. Tang and Y. Zhang, *Environ. Sci. Pollut. Res.*, **25**, 1405 (2018).
16. F. Reguyal, A. K. Sarmah and W. Gao, *J. Hazard. Mater.*, **321**, 868 (2017).
17. D. G. Kim, D. Choi, S. Cheon, S.-O. Ko, S. Kang and S. Oh, *J. Water Process Eng.*, **33**, 101019 (2020).
18. M. T. Sekulic, N. Boskovic, M. Milanovic, N. G. Letic, E. Gligoric and S. Pap, *J. Mol. Liq.*, **284**, 372 (2019).
19. M. Qi, Y. Yang, X. Zhang, X. Zhang, M. Wang, W. Zhang, X. Lu and Y. Tong, *J. Cleaner Prod.*, **253**, 120003 (2020).
20. L. Yan, Y. Liu, Y. Zhang, S. Liu, C. Wang, W. Chen, C. Liu, Z. Chen and Y. Zhang, *Bioresour. Technol.*, **297**, 122381 (2020).
21. J.-Y. Kim, S. Oh and Y.-K. Park, *J. Hazard. Mater.*, **384**, 121356 (2020).
22. S. Valizadeh, S. S. Lee, Y. J. Choi, K. Baek, B.-H. Jeon, K.-Y. Andrew Lin and Y.-K. Park, *Environ. Res.*, **213**, 113599 (2022).
23. W. Feng, Y. Ye, Z. Lei, C. Feng, C. Wei and S. Chen, *Carbon*, **134**, 53 (2018).
24. L. Tang, J. Yu, Y. Pang, G. Zeng, Y. Deng, J. Wang, X. Ren, S. Ye, B. Peng and H. Feng, *Chem. Eng. J.*, **336**, 160 (2018).
25. Y. Ma, L. Yang, L. Wu, P. Li, X. Qi, L. He, S. Cui, Y. Ding and Z. Zhang, *Sci. Total Environ.*, **718**, 137299 (2020).
26. J. Wan, J. Ding, W. Tan, Y. Gao, S. Sun and C. He, *Environ. Sci. Pollut. Res. Int.*, **27**, 13436 (2020).
27. H. Wang, X. Lou, Q. Hu and T. Sun, *J. Mol. Liq.*, **325**, 114967 (2021).
28. H. D. Liu, G. R. Xu and G. B. Li, *Sci. Total Environ.*, **747**, 141492 (2020).
29. Y. Yang, L. Zheng, T. Zhang, H. Yu, Y. Zhan, Y. Yang, H. Zeng, S. Chen and D. Peng, *Bioresour. Technol.*, **288**, 121510 (2019).
30. A. Fernandez-Sanroman, V. Acevedo-García, M. Pazos, M. A. Sanromán and E. Rosales, *J. Cleaner Prod.*, **271**, 122436 (2020).
31. R. Rashid, I. Shafiq, M. J. Iqbal, M. Shabir, P. Akhter, M. H. Hamayun, A. Ahmed and M. Hussain, *J. Environ. Chem. Eng.*, **9**, 105480 (2021).
32. Y. Ma, T. Lu, L. Yang, L. Wu, P. Li, J. Tang, Y. Chen, F. Gao, S. Cui, X. Qi and Z. Zhang, *Environ. Pollut.*, **298**, 118833 (2022).
33. Y. Ma, T. Lu, J. Tang, P. Li, O. Mašek, L. Yang, L. Wu, L. He, Y. Ding, F. Gao, X. Qi and Z. Zhang, *Sep. Purif. Technol.*, **297**, 121426 (2022).
34. Z. Zhang, Y. Li, L. Ding, J. Yu, Q. Zhou, Y. Kong and J. Ma, *Bioresour. Technol.*, **330**, 124949 (2021).
35. E. Smidt and V. Parravicini, *Bioresour. Technol.*, **100**, 1775 (2009).
36. K. Azam, R. Raza, N. Shezad, M. Shabir, W. Yang, N. Ahmad, I. Shafiq, P. Akhter, A. Razzaq and M. Hussain, *J. Environ. Chem. Eng.*, **8**, 104220 (2020).
37. V.-T. Nguyen, T.-B. Nguyen, C. P. Huang, C.-W. Chen, X.-T. Bui and C.-D. Dong, *J. Water Process Eng.*, **40**, 101908 (2021).
38. X. B. Zhang, Y. C. Zhang, H. H. Ngo, W. S. Guo, H. T. Wen, D. Zhang, C. C. Li and L. Qi, *Sci. Total Environ.*, **716**, 137015 (2020).
39. Y. Zhou, Y. He, Y. He, X. Liu, B. Xu, J. Yu, C. Dai, A. Huang, Y. Pang and L. Luo, *Sci. Total Environ.*, **650**, 2260 (2019).
40. J. Yan, Y. Xue, L. Long, Y. Zeng and X. Hu, *Environ. Sci. Pollut. Res.*, **25**, 34674 (2018).
41. C. Peiris, S. R. Gunatilake, T. E. Mlsna, D. Mohan and M. Vithanage, *Bioresour. Technol.*, **246**, 150 (2017).
42. S. Zeng, Y.-K. Choi and E. Kan, *Sci. Total Environ.*, **750**, 141691 (2021).
43. J. Wei, Y. Liu, J. Li, Y. Zhu, H. Yu and Y. Peng, *Chemosphere*, **236**, 124254 (2019).
44. Y. Liu, X. H. Liu, G. D. Zhang, T. Ma, T. Q. Du, Y. Yang, S. Y. Lu and W. L. Wang, *Colloids Surf., A*, **564**, 131 (2019).
45. X. Lin, J. Zhang, X. Luo, C. Zhang and Y. Zhou, *Chem. Eng. J.*, **172**, 856 (2011).
46. Y. Ma, P. Li, L. Yang, L. Wu, L. He, F. Gao, X. Qi and Z. Zhang, *Ecotoxicol Environ. Saf.*, **196**, 110550 (2020).
47. X. Fan, X. Wang, B. Zhao, J. Wan, J. Tang and X. Guo, *J. Environ. Chem. Eng.*, **10**, 107328 (2022).
48. F. Liu, J. Liu, Y. Li, R. Fang and Y. Yang, *Energy*, **239**, 122100 (2022).
49. A. K. De and I. Sinha, *J. Phys. Chem. Solids*, **167**, 110733 (2022).
50. A. R. Altaf, Y. G. Adewuyi, H. Teng, G. Liu and F. Abid, *J. Environ. Sci.*, **122**, 150 (2022).
51. X. Cao, Z. Meng, E. Song, X. Sun, X. Hu, L. Wenbin, Z. Liu, S. Gao and B. Song, *Chemosphere*, **299**, 134414 (2022).
52. Q. Wang, Z. Zhang, G. Xu and G. Li, *J. Hazard. Mater.*, **413**, 125385 (2021).
53. Q. Xu, Q. Zhou, M. Pan and L. Dai, *Chem. Eng. J.*, **382**, 122705 (2020).
54. F. Li, A. R. Zimmerman, X. Hu and B. Gao, *Chemosphere*, **260**, 127610 (2020).
55. Z. Peng, Z. Fan, X. Chen, X. Zhou, Z. F. Gao, S. Deng, S. Wan, X. Lv, Y. Shi and W. Han, *Nanomaterials*, **12**, 2271 (2022).
56. M. B. Ahmed, J. L. Zhou, H. H. Ngo, W. Guo, M. A. H. Johir and D. Belhaj, *Bioresour. Technol.*, **238**, 306 (2017).
57. C. E. Rodriguez-Martinez, E. Gutierrez Segura, C. Fall and A. Colin-Cruz, *Desalin. Water Treat.*, **158**, 67 (2019).